
Parabolic Approximation Line Search for DNNs

Maximus Mutschler and Andreas Zell

University of Tübingen

Sand 1, D-72076 Tübingen, Germany

{maximus.mutschler, andreas.zell}@uni-tuebingen.de

Abstract

A major challenge in current optimization research for deep learning is to automatically find optimal step sizes for each update step. The optimal step size is closely related to the shape of the loss in the update step direction. However, this shape has not yet been examined in detail. This work shows empirically that the sample loss over lines in negative gradient direction is mostly convex and well suited for one-dimensional parabolic approximations. Exploiting this parabolic property we introduce a simple and robust line search approach, which performs loss-shape dependent update steps. Our approach combines well-known methods such as parabolic approximation, line search and conjugate gradient, to perform efficiently. It successfully competes with common and state-of-the-art optimization methods on a large variety of experiments without the need of hand-designed step size schedules. Thus, it is of interest for objectives where step-size schedules are unknown or do not perform well. Our excessive evaluation includes multiple comprehensive hyperparameter grid searches on several datasets and architectures. We provide proof of convergence for an adapted scenario. Finally, we give a general investigation of exact line searches in the context of sample losses and exact losses, including their relation to our line search approach.

1 Introduction

Automatically finding the optimal step sizes for each update step of stochastic gradient descent is one major challenge in current optimization research for deep learning [2, 4, 11, 28, 36, 39, 42, 46, 54]. One default approach to tackle this challenge is to apply line searches. Several of these have been introduced for Deep Learning [11, 28, 36, 39, 54]. However, these approaches have not analyzed the shape of the loss functions in update step direction, which is important, since the optimal step size stands in strong relation to it. To shed light on this, our work empirically analyses the shape of the loss function in update step direction for deep learning scenarios often considered in optimization. We further elaborate the properties found to define a simple, competitive, state-of-the-art optimizer. Our contributions are as follows: **1:** Our empirical analysis suggests that the loss function in negative gradient direction mostly shows locally convex shapes. Furthermore, we show that parabolic approximations are well suited to estimate the minima in these directions (Section 3). **2:** Exploiting the parabolic property, we build a simple state-of-the-art line search optimizer which realizes its own loss function dependent learning rate schedule. The performance of our optimization method is extensively analyzed, including a comprehensive comparison to other optimization methods (Sections 4,5). **3:** We provide a convergence analysis which fits to our empirical results with some assumptions (Section 4.4). **4:** Finally, we provide a general investigation of exact line searches on sample losses and their relation to line searches on the exact loss as well as their relation to our line search approach (Section 6).

The empirical loss function \mathcal{L} is generally defined as the average over a batch-wise loss function L : $\mathcal{L}(x; \theta) : \mathbb{R}^n \rightarrow \mathbb{R}, x \mapsto n^{-1} \sum_{i=1}^n L(x_i; \theta)$ with n being the amount of batches, x_i defining a sample (batch) and θ being the parameters to be optimized. Note that we see one sample as one batch

of multiple inputs. We call $L(x_t; \theta)$ the sample loss for sample x at optimization step t . In this work, we consider $L(x_t; \theta)$ in negative gradient direction:

$$l_t(s) : \mathbb{R} \rightarrow \mathbb{R}, s \mapsto L(x_t; \theta_t + s \cdot \frac{-g_t}{\|g_t\|}) \quad (1)$$

where g_t is defined as $\nabla_{\theta_t} L(x_t; \theta_t)$. For simplification we call $l_t(s)$ a line and s a step on the line. Following [2] implicitly, the motivation of our work builds upon the following assumption:

Assumption 1. (Informal) The position $\theta_{min} = \theta_t + s_{min} \frac{-g_t}{\|g_t\|}$ of a minimum on l_t is a well enough estimator for the position of the minimum of the empirical loss \mathcal{L} on the same line to perform a successful optimization process.

We will analyze Assumption 1 further in section 6.

2 Related Work

Our optimization approach is based on well-known methods such as line search, the non linear conjugate gradient method and quadratic approximation, which can be found in Numerical Optimization [27]. Our work contrasts all other approaches by directly and simply exploiting the parabolic property (see Section 3) of lines of the sample loss.

The recently published *Stochastic Line-Search (SLS)* [54] is an optimized backtracking line search based on the Armijo condition, which samples, like our approach, additional sample losses from the same batch and checks the Armijo condition on these. Thus, [54] follows a similar but weaker assumption than Assumption 1: [54] assumes that a position θ that fulfills the Armijo condition on the sample loss line is also a good position on the corresponding empirical loss line. *SLS* shows competitive performance against multiple optimizers on several DNN tasks. [39] introduces a similar idea, but, does not provide empirical results for DNNs. The beautiful but complex *Probabilistic Line Search (PLS)* [36] and *Gradient Only Line Search (GOLSI)* [28] are considering a discontinuous stochastic loss function. *GOLSI* searches for a minimum on lines by searching for a sign change of the first directional derivative in search direction. *PLS* optimizes on lines of a stochastic loss function by approximating it with a Gaussian Process surrogate and exploiting a probabilistic formulation of the Wolf conditions. Both approaches show that they can optimize successfully on several machine learning problems and can compete against plain *SGD*. [9] explores a similar direction as this work by analyzing possible line search approximations for DNNs. [11] regulates the optimal batch size with a backtracking Armijo line search. Indirectly *SGD-HD* [2] also searches for the minimum position of lines.

From the perspective of assumptions about the shape of the loss landscape, second order methods such as *oLBFGS* [49], *KFRA* [6], *L-SRI* [41], *QUICKPROP* [14], *S-LSRI* [3], and *KFAC* [37] generally assume that the loss function can be approximated locally by a parabola of the same dimension as the loss function. Adaptive methods such as *SGD* with momentum [45], *ADAM* [29], *ADAGRAD* [13], *ADABOUND* [35], *AMSGRAD* [43] or *RMSPprop* [53] concentrate more on the handling of noise than on shape assumptions. In addition, methods exist that approximate the loss function in specific directions: The *L4* adaptation scheme [46] as well as [4] approximate the loss function linearly in negative gradient direction, whereas our approach approximates the loss function parabolically in negative gradient direction.

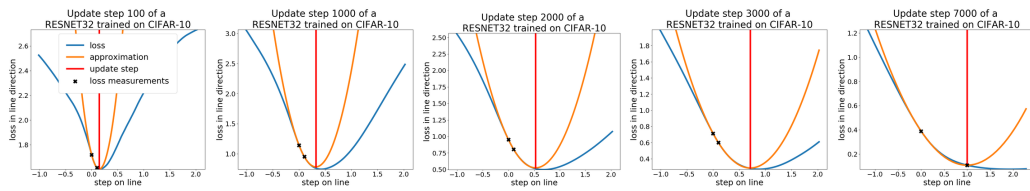


Figure 1: Sample losses on lines in negative normalized gradient direction (blue), parabolic approximations (orange) and the position of the approximated minima (red). Further line plots are provided in Appendix A.

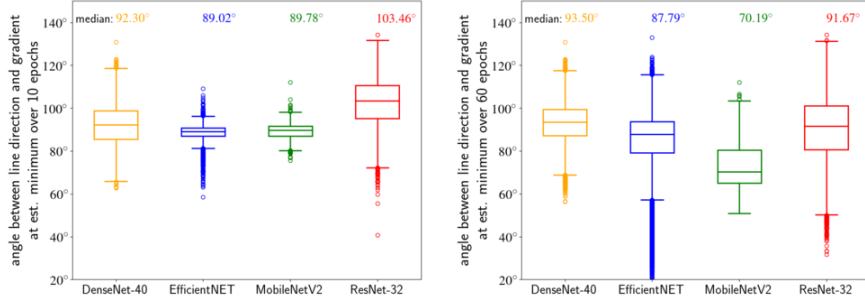


Figure 2: Angles between the line direction and the gradient at the estimated minimum measured on the same batch. If the angle is 90° , the estimated minimum is a real local minimum. We know from additional line plots that the found extrema or saddle points are minima. Left: measurement over the first 10 epochs. Right: measurement over the first 60 epochs. Update step adaptation (see Section 4.3) is applied.

3 Empirical analysis of the shape of sample loss lines

In this section we analyze lines (see Eq. 1) during the training of multiple architectures and show that they are mostly convex and well suited for parabolic approximations. We focus on CIFAR-10, as it is extensively analyzed in optimization research for deep learning. However, on random samples of CIFAR-100, Imagenet and Tolstoi we observed the same. We analyzed the lines of 4 common used architectures in detail. To do so, we evaluated the lines of the first 10000 update steps for each architecture. For each line we sampled 50 losses and performed a parabolic approximation (see Section 4). An unbiased selection of our results on a ResNet32 is shown in Figure 1. Further results are given in Appendix A. In accordance with [55], we conclude that the analyzed lines tend to be locally convex. In addition, one-dimensional parabolic approximations of the form $f(s) = as^2 + bs + c$ with $a \neq 0$ are well suited to estimate the position of a minimum on such lines. To substantiate the later observation, we analyzed the angle between the line direction and the gradient at the estimated minimum during training with parabolic approximations. A position is a local extremum or saddle point of the line if and only if the angle between the line direction and the gradient at the position is 90° when measured on the same batch.¹ As shown in Figure 2 (left), this property holds well for the first 10 epochs with several architectures trained on CIFAR-10. Figure 2 (right) shows that the property tends to become slightly less accurate when training is continued for additional 50 epochs. One reason for this is, that the local shapes of the lines tend to form flatter regions around the minimum when training progresses, as shown exemplary in the last line plot of Figure 1. We can ensure that the extrema found are minima, since we additionally plotted the loss line for each update step.

4 The line search algorithm

By exploiting the property, that parabolic approximations are well suited to estimate the position of minima on lines, we introduce **Parabolic Approximation Line Search (PAL)**. This simple approach combines well-known methods from basic optimization such as parabolic approximation, line search and conjugate gradient [27], to perform an efficient line search. We note, that the general idea of this method can be applied to any optimizer which provides an update step direction.

4.1 Parameter update rule

An intuitive explanation of *PAL*'s parameter update rule based on a parabolic approximation is given in Figure 3. Since $l_t(s)$ (see Eq.1) is assumed to be a parabolic function, it has the form $l_t(s) = as^2 + bs + c$ with $a \neq 0$ and $a, b, c \in \mathbb{R}$. We need three measurements to define a, b and c .

¹This holds because if the directional derivative of the measured gradient in direction of the line is 0, the current position is an extremum or saddle point of the line and the angle is 90° . If the position is not a extremum or saddle point, the directional derivative is not 0 [27].

Those are given by the current loss $l_t(0)$, the derivative in gradient direction $l'_t(0) = -\|g_t\|$ (see Eq. 4) and an additional loss $l_t(\mu)$ with measuring distance $\mu \in \mathbb{R}^+$. We get $a = \frac{l_t(\mu) - l_t(0) - l'_t(0)\mu}{\mu^2}$, $b = l'_t(0)$, and $c = l_t(0)$. The update step s_{upd} to the minimum of the parabolic approximation is thus given by:

$$s_{upd_t} = -\frac{l'_t(0)}{l''_t(0)} = -\frac{b}{2a} = \frac{-l'_t(0)}{2 \frac{l_t(\mu) - l_t(0) - l'_t(0)\mu}{\mu^2}} \quad (2)$$

Note that $l''_t(0)$ is the second derivative of the approximated parabola and is only identical to the exact directional derivative $\frac{-g_t}{\|g_t\|} H(L(x_t; \theta_t)) \frac{-g_t^T}{\|g_t\|}$ if the parabolic approximation fits. The normalization of the gradient to a length of 1 (Eq.1) was chosen to have the measuring distance μ independent of the gradient size. Note that two network inferences are required to determine $l_t(0)$ and $l_t(\mu)$. Thus, *PAL* needs two forward passes and one backward pass through a network. Further on, the sample loss $L(x_t; \theta_t)$ may include random components, but, to ensure continuity during one line search, drawn random numbers have to be reused for each value determination of L at t (e.g. for Dropout). The memory required by *PAL* is similar to *SGD* with momentum, since only the last update direction has to be saved. A basic, well performing version of *PAL* is given in Algorithm 1.

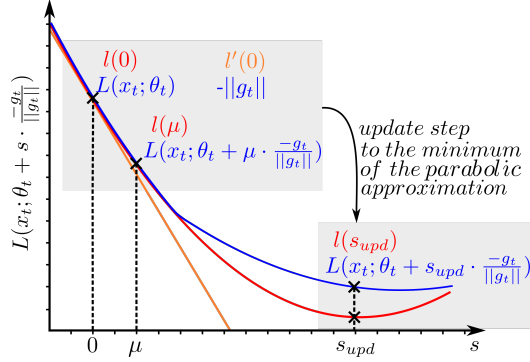


Figure 3: Basic idea of *PAL*'s parameter update rule. The blue curve is the loss function on a line in direction of the negative gradient at $L(x_t; \theta_t)$. It is defined by $l(s) = L(x_t; \theta_t + s \cdot \frac{-g_t}{\|g_t\|})$ where g_t is $\nabla_{\theta_t} L(x_t; \theta_t)$. The red curve is its parabolic approximation. With $l(0)$, $l(\mu)$ and g_t (orange), we have the three parameters needed to determine the update step s_{upd} to the minimum of the parabolic approximation.

4.2 Case discrimination of parabolic approximations

Since not all parabolic approximations are suitable for parameter update steps, the following cases are distinguished. Note that $b = l'_t(0)$ and $a = 0.5l''_t(0)$. **1:** $a > 0$ and $b < 0$: parabolic approximation has a minimum in line direction. Parameter update is done as described in Section 4.1. **2:** $a \leq 0$ and $b < 0$: parabolic approximation has a maximum in negative line direction, or is a line with negative slope. In those cases a parabolic approximation is inappropriate. s_{upt} is set to μ , since the second measured point has a lower loss as the first. **3:** Since $b = -\|g_t\|$ cannot be greater than 0, the only case left is an extremum at the current position ($l'(0) = 0$). In this case, no weight update is performed. However, the loss function is changed by the next batch. In accordance to Section 3, cases 2 and 3 appear very rarely in our experiments.

Algorithm 1 The basic version of our proposed line search algorithm. See Section 4 for details.

<p>Input: μ: measuring step size</p> <p>Input: $L(x; \theta)$: loss function</p> <p>Input: x: list of input vectors</p> <p>Input: θ_0: initial parameter vector</p> <p>1: $t \leftarrow 0$</p> <p>2: while θ_t not converged do</p> <p>3: $l_0 \leftarrow L(x_t; \theta_t)$ # $l_0 = l_t(0)$ see Eq. 1</p> <p>4: $g_t \leftarrow -\nabla_{\theta_t} L(x_t; \theta_t)$</p> <p>5: $l_\mu \leftarrow L(x_t; \theta_t + \mu \frac{g_t}{\ g_t\ })$</p> <p>6: $b \leftarrow -\ g_t\$</p>	<p>7: $a \leftarrow \frac{l_\mu - l_0 - b\mu}{\mu^2}$</p> <p>8: if proper curvature then</p> <p>9: $s_{upd} \leftarrow -\frac{b}{2a}$</p> <p>10: else</p> <p>11: # set s_{upd} according to section 4.2</p> <p>12: end if</p> <p>13: $\theta_{t+1} \leftarrow \theta_t + s_{upd} \frac{g_t}{\ g_t\ }$</p> <p>14: $t \leftarrow t + 1$</p> <p>15: end while</p> <p>16: return θ_t</p>
--	---

4.3 Additions

We introduce multiple additions for Algorithm 1 to fine tune the performance and handle degenerate cases. We emphasize that our hyperparameter sensitivity analysis (Appendix D.4) suggests that the influence of the introduced hyperparameters on the optimizer’s performance are low. Thus, they only need to be adapted to fine tune the results. The full version of *PAL* including all additions is given in Algorithm 2 (Appendix).

Conjugate gradient: Instead of following the direction of the negative gradient we follow a conjugate direction d_t :

$$d_t = -\nabla_{\theta_t} L(x_t; \theta_t) + \beta d_{t-1} \quad d_0 = -\nabla_{\theta_0} L(x_0; \theta_0) \quad (3)$$

with $\beta \in [0, 1]$. Since we now use a conjugate direction, $l'_t(0)$ changes to:

$$l'_t(0) = \nabla_{\theta_t} L(x_t; \theta_t) \frac{d_t}{\|d_t\|} \quad (4)$$

This approach is used to find a more optimal search direction than the negative gradient. We implemented and tested the formulas of Fletcher-Reeves [15], Polak-Ribière [44], Hestenes-Stiefel [23] and Dai-Yuan [10] to determine a good β for each time step t . However, choosing a constant β of value 0.2 or 0.4 performs equally well. For a slight speedup, one could approximate $l'(0)$ with $\|d_t\|$.

Update step adaptation: Our preliminary experiments revealed a systematic error of constantly approximating with slightly too narrow parabolas. Therefore, s_{upd} gets multiplied by a parameter $\alpha \geq 1$ (compare to Eq. 2). This is useful to estimate the position of the minimum on a line more exact, but has minor effect on training performance.

Maximum step size: To hinder the algorithm from failing due to inaccurate parabolic approximations, we use a maximum step size s_{max} . The new update step is given by $\min(s_{upd}, s_{max})$. However, most of our experiments with $s_{max} = 10^{0.5} \approx 3.16$ never reached this step size and still performed well.

4.4 Theoretical Analysis

This section provides a convergence analysis based on the assumption that each slice of the loss function is a one-dimensional parabolic function:

Assumption 2. Let $n \in \mathbb{N}$ be the number of parameters and let $\mathbf{l}, \mathbf{d} \in \mathbb{R}^n$ be vectors. Then for all \mathbf{l}, \mathbf{d} there exists $a, b, c \in \mathbb{R}$ with $a > 0$, such that $L(x_t; \mathbf{l} + \mathbf{d}s) = as^2 + bs + c$ for all $s \in \mathbb{R}$.

This assumption is a simplified adaptation to our empirical results that lines in negative gradient direction behave locally almost parabolic (see Section 3). For the following derivations we assume a basic *PAL* without the additions introduced in Section 4.3. Proofs are provided in Appendix C. At first we show that $L(x_t, \theta)$ is a n-dimensional parabolic function:

Lemma 1. Let $f : \mathbb{R}^n \rightarrow \mathbb{R}$ be a k -times continuously differentiable function. Furthermore, assume there exists $a, b, c \in \mathbb{R}$ with $a > 0$, such that $f(\mathbf{l} + \mathbf{d}s) = as^2 + bs + c$ for all $s \in \mathbb{R}$. Then there exist $z \in \mathbb{R}, \mathbf{r} \in \mathbb{R}^n$ and a positive definite Matrix $\mathbf{Q} \in \mathbb{R}^{n \times n}$ such that $f(\mathbf{x}) = c + \mathbf{r}^T \mathbf{x} + \mathbf{x}^T \mathbf{Q} \mathbf{x}$ for all $\mathbf{x} \in \mathbb{R}^n$.

Now we show that *PAL* converges on $L(x_t, \theta)$:

Proposition 1. *PAL* converges on $f(\mathbf{x}) : \mathbb{R}^n \rightarrow \mathbb{R}, f(\mathbf{x}) = c + \mathbf{r}^T \mathbf{x} + \mathbf{x}^T \mathbf{Q} \mathbf{x}$ with $\mathbf{Q} \in \mathbb{R}^{n \times n}$ hermitian and positive definite.

However, for a noisy scenario where each batch defines a parabolic function, *PAL* has no convergence guarantee. Given two shifted one-dimensional parabolas, $ax^2 + bx + c$ and $a(x+d)^2 + b(x+d) + c$, which are presented to *PAL* alternately, *PAL* will always perform an update step to the minimum position of one of these but never to the minimum position of the average of both. By changing the training procedure and assuming that each $L(x_i, \theta)$ has the same \mathbf{Q} this can be fixed:

Proposition 2. If $\mathcal{L}(\theta) : \mathbb{R}^n \rightarrow \mathbb{R} \theta \mapsto \mathcal{L}(\theta) = \frac{1}{m} \sum_{i=1}^m c_i + \mathbf{r}_i^T \theta + \theta^T \mathbf{Q}_i \theta$ and $c_i + \mathbf{r}_i^T \theta + \theta^T \mathbf{Q}_i \theta = L(\theta; \mathbf{x}_i)$ with m being number the of batches and \mathbf{x}_i defining one batch. (Each batch defines a parabola. The empirical loss $\mathcal{L}(\theta)$ is the mean of these parabolas). And for all $i, j \in \mathbb{N}$ it holds that $\mathbf{Q}_i = \mathbf{Q}_j$ and that \mathbf{Q}_i is positive definite. Then $\arg \min_{\theta} \mathcal{L}(\theta) = \frac{1}{m} \sum_{i=1}^m \arg \min_{\theta} L(\theta)$ holds.

This means that under Assumption 2 and a fixed \mathbf{Q} the position of the minimum of the empirical loss is given by the average of the positions of the minima of the sample losses. The minimum position of the empirical loss is found by *PAL*, by slightly adapting *PAL* to search on one batch until it finds the position of the minimum and then averaging the minima of each batch. As a result, *PAL* converges in this noisy scenario. However, we have to emphasize at this point that our assumption about \mathbf{Q} is likely not valid for general deep learning scenarios. But, if it is locally valid, this direction might be a further explanation, in addition to those of [16, 21], why stochastic weight averaging [25] performs well.

5 Evaluation

5.1 Experimental Design

We performed a comprehensive evaluation to analyze the performance of *PAL* on a variety of deep learning optimization tasks. Therefore, we tested *PAL* on multiple state-of-the-art or commonly used architectures on CIFAR-10 [30], CIFAR-100 [30] and Imagenet [12]. For CIFAR-10 and CIFAR-100, we evaluated on DenseNet40 [24], EfficientNetB0 [52], ResNet32 [22] and MobileNetV2 [48]. On Imagenet we evaluated on DenseNet121 and ResNet50. In addition, we evaluated on an RNN trained on the Tolstoi war and peace text prediction task. We compare *PAL* to *SLS* [54], whose Armijo variant is state-of-the-art in the line search field for DNNs. Furthermore, we compare *PAL* to the following well studied and widely used first order optimizers: *SGD* with momentum [45], *ADAM* [29] and *RMSProp* [53]. To perform a fair comparison, we compared a variety of hyperparameter combinations of commonly used hyperparameters for each optimizer. In addition, we utilize those combinations, to analyze the hyperparameter sensitivity for each optimizer. Since a grid search on Imagenet was too expensive, the best hyperparameter configuration from the CIFAR-100 evaluation was used to test hyperparameter transferability. A detailed explanation of the experiments including hyperparameters and data augmentations used are given in Appendix D.5. All in all, we trained 1494 networks with Tensorflow 1.15 [1] on Nvidia Geforce GTX 1080 TI graphic cards. Since *PAL* is a line search approach, the predefined learning rate schedules of *SGD* and the generated schedules of *SLS* and *PAL* are compared. Due to normalization, *PAL*'s learning rate is given by $s_{upd_t}/||d_t||$.

5.2 Results

The results of our comparison on DenseNets are given in Figure 4. The results on other architectures trained on CIFAR-10, CIFAR-100, Imagenet and Tolstoi are found in Appendix D Figures 11,12. A table with exact numerical results of all experiments is provided in Appendix D.6.

In most cases *PAL* decreases the training loss faster and to a lower value than the first order optimizers (row 1 of Figures 4,11,12). Considering validation and test accuracy *PAL* competes with *RMSProp* and *ADAM* but gets surpassed by *SGD* (rows 2,3 of Figures 4,11,12). However, those optimizers were tuned by a good step size schedule. If we compare *PAL* to their basic implementations without a schedule, which roughly corresponds to the first plateau reached in row 2 of Figures 4,11,12, *PAL* would surpass the other optimizers and shows that it can find a well performing step size schedule. This is especially interesting for problems where default schedules might not work.

SLS decreases the training loss further than the other optimizers on a few problems, but shows weak performance on most. In addition, it generalizes worse. This contrasts to the results of [54], where *SLS* behaves robustly and excels. To exclude the possibility of errors on our side, we reimplemented *SLS* experiment on ResNet34 and could reach a similar well performance as in [54] (Appendix D.1). Considering the box plots of Figures 4 and 11, which represent the sensitivity to hyperparameter combinations one would likely try on a new unknown objective, we can see, that *PAL* has a strong tendency to be less sensitive. To emphasize this statement, a sensitivity analysis of *PAL*'s hyperparameters (Appendix Figure 14) shows that *PAL* performs well on a wide range for each hyperparameter when training a ResNet32 on CIFAR-10.

On wall-clock-time *PAL* performs as fast as *SLS* but slower than *SGD* (Appendix D.2). However, depending on the scenario, an automatic, well performing leaning rate schedule might outweigh the slower speed.

Considering the learning rate schedules of *PAL* (row 4 of Figures 4,11,12) we achieved unexpected results. *PAL*, which estimates the learning rate directly from approximated local shape information, does not follow a schedule that is similar to the one of *SLS* or any of the common used hand crafted schedules such as piece wise constant or cosine decay . However, it achieves similar results.

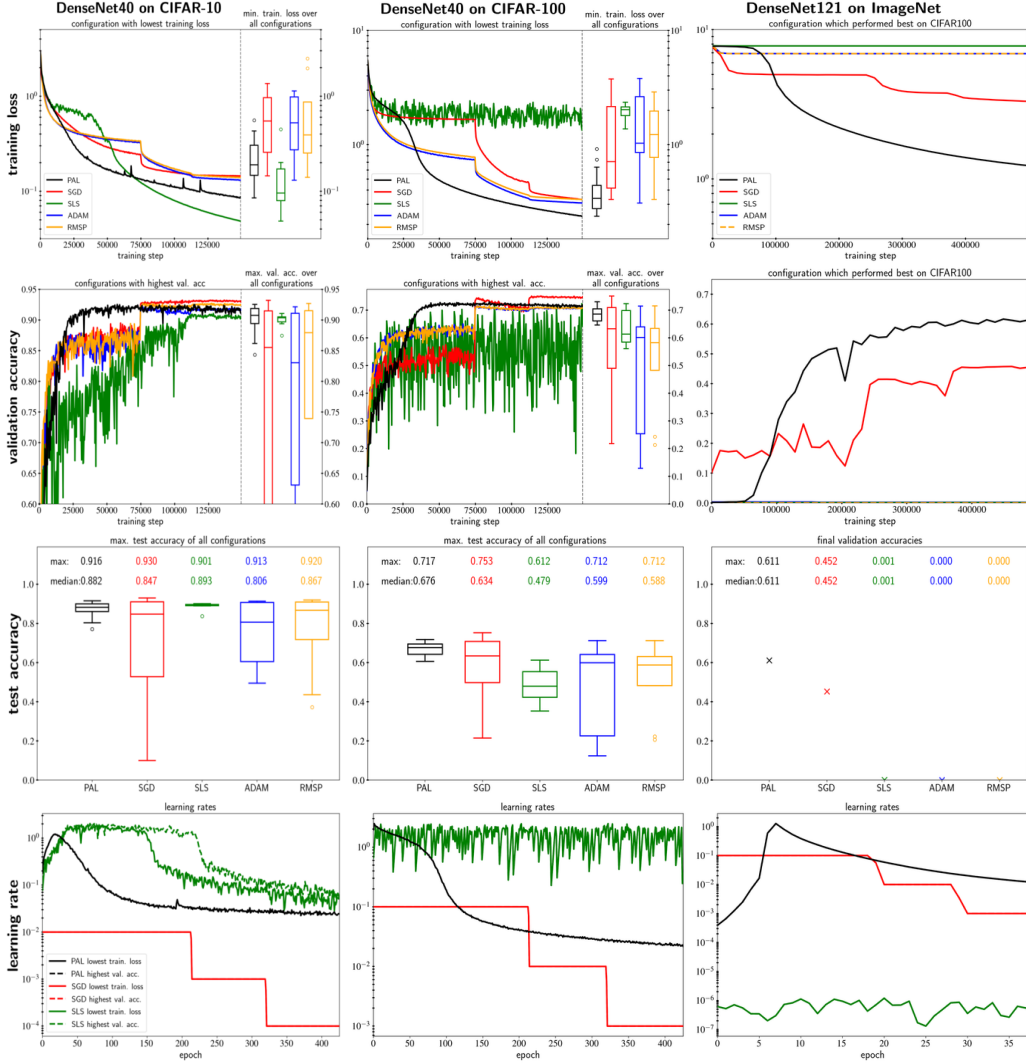


Figure 4: Comparison of *PAL* against *SLS*, *SGD*, *ADAM*, *RMSProp* on train. loss (row 1), val. acc. (row 2), test. acc. (row 3) and *SLS*, *SGD* and *PAL* on learning rates (row 4). Comparison is done on **DenseNets** on different Datasets. Results are averaged over 3 runs. Box plots result from comprehensive hyperparameter grid searches in plausible intervals. For Imagenet the best hyperparameter configuration from the CIFAR-100 evaluation were used to test hyperparameter transferability.

Our results show, that *PAL* is a robust line search approach, and might be used as an alternative to *SGD* for problems where default step size schedules might fail.

6 On the exactness of line searches on sample losses

In this section we investigate the general questions if line searches which are estimating the location of the minimum exactly are beneficial. In Figure 2 we showed that *PAL* can perform an almost exact line search on sample losses if we use a fixed update step adaptation (Section 4.3) factor. However, *PAL*'s best hyperparameter configuration does not perform an exact line search (Figure 5). Thus, we analyzed, how an exact line search which exactly estimates a minimum of the line behaves. We implemented an inefficient binary line search (Appendix E), which measured up to 20 values on each line to estimate the position of a minimum. The results, given in Figure 5, show that an optimal line search does not optimize well. Thus, the reason why *PAL* performs well is not the exactness of its update steps. In fact, slightly inexact update steps seem to be beneficial.

Those results query Assumption 1, which assumes that the position of a minimum on a line in negative gradient direction of the sample loss $L(x_t; \theta)$ is a well enough estimator for the minimum of the

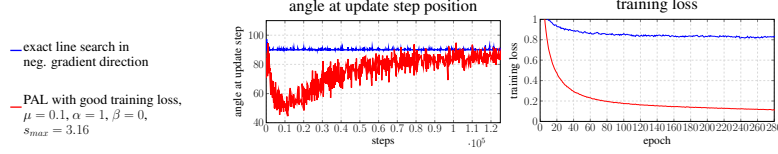


Figure 5: Comparison of *PAL* against an expensive exact line search. The first plot shows the angle between the direction and gradient vector at the update step position. The training was performed with a ResNet32 on CIFAR-10. One can observe that an exact line search does not perform well.

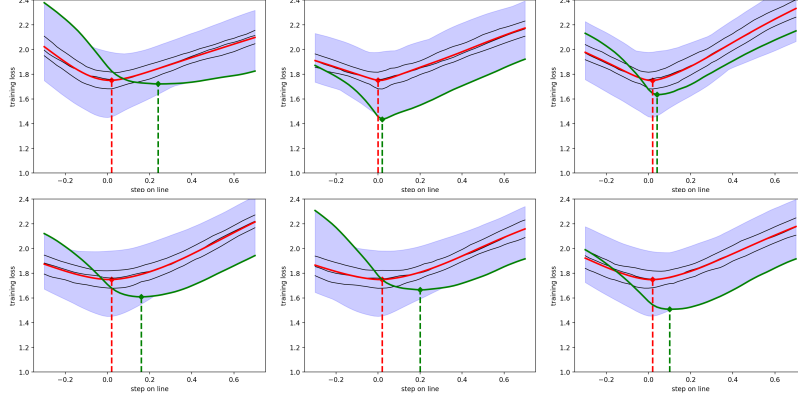


Figure 6: Distributions (blue) over all sample losses on representative lines during a training process of a ResNet32 on CIFAR-10. The empirical loss, which is the mean value of the distribution, is given in red. The quartiles are given in black. The sample loss, whose negative gradient defines the search direction, is given in green. It can be observed that the minimum of the green sample loss is not always a good estimator of the minimum of the empirical loss on the corresponding line.

empirical loss \mathcal{L} on this line to perform a successful optimization process. To investigate this further, we tediously measured the empirical loss $\mathcal{L}(\theta_t)$ and the distribution of sample losses for one training process on a ResNet32. Our results suggest, as exemplary shown in Figure 6, that on a line defined by the gradient of $L(x_t; \theta)$, the position of the minimum of $L(x_t; \theta)$ is not always a good estimator for the position of the minimum of the empirical loss \mathcal{L} , which explains why exact line searches on the sample loss perform weak. Corollaries are that the empirical loss on the investigated lines also tends to be locally convex and that the optimal step size tends to be smaller than the step size given by the sample loss on such lines. This is a possible explanation why the slightly too narrow parabolic approximations of *PAL* without update step adaptation perform well.

7 Conclusions

This work tackles a major challenge in current optimization research for deep learning: to automatically find optimal step sizes for each update step. In detail, we focus on line search approaches to deal with this challenge. We introduced a simple, robust and competitive line search approach based on one-dimensional parabolic approximations. The introduced algorithm is an alternative to *SGD* for objectives where default decays are unknown or do not work.

Loss functions of DNNs are commonly perceived as being highly non-convex. Our analysis suggests that this intuition does not hold locally, since lines of loss landscapes across models and datasets can be approximated parabolically to high accuracy. This new knowledge might further help to explain, why update steps of specific optimizers perform well.

To gain a deeper understanding of line searches in general, we analyzed how an expensive but exact line search on sample losses behaves. Surprisingly, its performance is weak, which lets us conclude that the small inaccuracies of the parabolic approximations are beneficial for training.

Potential broader impact: Since we understand our work as basic research, it is extremely error-prone to estimate its *specific* ethical aspects and future positive or negative social consequences. As optimization research influences the whole field of deep learning, we refer to the following works, which discuss the ethical aspects and social consequences of AI and Deep Learning in a comprehensive and general way: [5, 38, 57].

References

- [1] M. Abadi, A. Agarwal, P. Barham, E. Brevdo, Z. Chen, C. Citro, G. S. Corrado, A. Davis, J. Dean, M. Devin, S. Ghemawat, I. Goodfellow, A. Harp, G. Irving, M. Isard, Y. Jia, R. Jozefowicz, L. Kaiser, M. Kudlur, J. Levenberg, D. Mané, R. Monga, S. Moore, D. Murray, C. Olah, M. Schuster, J. Shlens, B. Steiner, I. Sutskever, K. Talwar, P. Tucker, V. Vanhoucke, V. Vasudevan, F. Viégas, O. Vinyals, P. Warden, M. Wattenberg, M. Wicke, Y. Yu, and X. Zheng. TensorFlow: Large-scale machine learning on heterogeneous systems, 2015. Software available from tensorflow.org.
- [2] A. G. Baydin, R. Cornish, D. M. Rubio, M. Schmidt, and F. Wood. Online learning rate adaptation with hypergradient descent. *arXiv preprint arXiv:1703.04782*, 2017.
- [3] A. S. Berahas, M. Jahani, and M. Takác. Quasi-newton methods for deep learning: Forget the past, just sample. *CoRR*, abs/1901.09997, 2019.
- [4] L. Berrada, A. Zisserman, and M. P. Kumar. Training neural networks for and by interpolation. *arXiv preprint arXiv:1906.05661*, 2019.
- [5] N. Bostrom and E. Yudkowsky. The ethics of artificial intelligence. *The Cambridge handbook of artificial intelligence*, 1:316–334, 2014.
- [6] A. Botev, H. Ritter, and D. Barber. Practical gauss-newton optimisation for deep learning. *arXiv preprint arXiv:1706.03662*, 2017.
- [7] A. Botev, H. Ritter, and D. Barber. Practical gauss-newton optimisation for deep learning. In *Proceedings of the 34th International Conference on Machine Learning-Volume 70*, pages 557–565. JMLR. org, 2017.
- [8] C.-A. Brust, S. Sickert, M. Simon, E. Rodner, and J. Denzler. Neither quick nor proper - evaluation of quickprop for learning deep neural networks. *CoRR*, abs/1606.04333, 2016.
- [9] Y. Chae and D. N. Wilke. Empirical study towards understanding line search approximations for training neural networks. *arXiv preprint arXiv:1909.06893*, 2019.
- [10] Y.-H. Dai and Y. Yuan. A nonlinear conjugate gradient method with a strong global convergence property. *SIAM Journal on optimization*, 10(1):177–182, 1999.
- [11] S. De, A. Yadav, D. Jacobs, and T. Goldstein. Big batch sgd: Automated inference using adaptive batch sizes. *arXiv preprint arXiv:1610.05792*, 2016.
- [12] J. Deng, W. Dong, R. Socher, L.-J. Li, K. Li, and L. Fei-Fei. ImageNet: A Large-Scale Hierarchical Image Database. In *CVPR09*, 2009.
- [13] J. Duchi, E. Hazan, and Y. Singer. Adaptive subgradient methods for on learning and stochastic optimization. *Journal of Machine Learning Research*, 12(Jul):2121–2159, 2011.
- [14] S. E. Fahlman et al. An empirical study of learning speed in back-propagation networks. 1988.
- [15] R. Fletcher and C. M. Reeves. Function minimization by conjugate gradients. *The computer journal*, 7(2):149–154, 1964.
- [16] S. Fort and S. Jastrzebski. Large scale structure of neural network loss landscapes. In *Advances in Neural Information Processing Systems*, pages 6706–6714, 2019.
- [17] X. Gastaldi. Shake-shake regularization. *CoRR*, abs/1705.07485, 2017.
- [18] X. Glorot and Y. Bengio. Understanding the difficulty of training deep feedforward neural networks. In *Proceedings of the thirteenth international conference on artificial intelligence and statistics*, pages 249–256, 2010.
- [19] I. J. Goodfellow, O. Vinyals, and A. M. Saxe. Qualitatively characterizing neural network optimization problems. *arXiv preprint arXiv:1412.6544*, 2014.
- [20] Google. Tensorflow adam optimizer documentation. https://www.tensorflow.org/api_docs/python/tf/train/AdamOptimizer. Accessed: 2019-11-12.
- [21] H. He, G. Huang, and Y. Yuan. Asymmetric valleys: Beyond sharp and flat local minima. In *Advances in Neural Information Processing Systems*, pages 2549–2560, 2019.
- [22] K. He, X. Zhang, S. Ren, and J. Sun. Deep residual learning for image recognition. In *Proceedings of the IEEE conference on computer vision and pattern recognition*, pages 770–778, 2016.
- [23] M. R. Hestenes and E. Stiefel. *Methods of conjugate gradients for solving linear systems*, volume 49. NBS Washington, DC, 1952.
- [24] G. Huang, Z. Liu, L. Van Der Maaten, and K. Q. Weinberger. Densely connected convolutional networks. In *CVPR*, volume 1, page 3, 2017.
- [25] P. Izmailov, D. Podoprikin, T. Garipov, D. Vetrov, and A. G. Wilson. Averaging weights leads to wider optima and better generalization. *arXiv preprint arXiv:1803.05407*, 2018.
- [26] P. Izmailov, D. Podoprikin, T. Garipov, D. Vetrov, and A. G. Wilson. Averaging weights leads to wider optima and better generalization. *arXiv preprint arXiv:1803.05407*, 2018.
- [27] S. W. Jorge Nocedal. *Numerical Optimization*. Springer series in operations research. Springer, 2nd ed edition, 2006.
- [28] D. Kafka and D. Wilke. Gradient-only line searches: An alternative to probabilistic line searches. *arXiv preprint arXiv:1903.09383*, 2019.
- [29] D. P. Kingma and J. Ba. Adam: A method for stochastic optimization. *CoRR*, abs/1412.6980, 2014.

- [30] A. Krizhevsky and G. Hinton. Learning multiple layers of features from tiny images. Technical report, Citeseer, 2009.
- [31] A. Krizhevsky, I. Sutskever, and G. E. Hinton. Imagenet classification with deep convolutional neural networks. In *Advances in neural information processing systems*, pages 1097–1105, 2012.
- [32] Y. A. LeCun, L. Bottou, G. B. Orr, and K.-R. Müller. Efficient backprop. In *Neural networks: Tricks of the trade*, pages 9–48. Springer, 2012.
- [33] H. Li, Z. Xu, G. Taylor, and T. Goldstein. Visualizing the loss landscape of neural nets. *CoRR*, abs/1712.09913, 2017.
- [34] L. Liu, H. Jiang, P. He, W. Chen, X. Liu, J. Gao, and J. Han. On the variance of the adaptive learning rate and beyond, 2019.
- [35] L. Luo, Y. Xiong, and Y. Liu. Adaptive gradient methods with dynamic bound of learning rate. In *International Conference on Learning Representations*, 2019.
- [36] M. Mahsereci and P. Hennig. Probabilistic line searches for stochastic optimization. *Journal of Machine Learning Research*, 18, 2017.
- [37] J. Martens and R. Grosse. Optimizing neural networks with kronecker-factored approximate curvature. In *International conference on machine learning*, pages 2408–2417, 2015.
- [38] L. Muehlhauser and L. Helm. The singularity and machine ethics. In *Singularity Hypotheses*, pages 101–126. Springer, 2012.
- [39] C. Paquette and K. Scheinberg. A stochastic line search method with convergence rate analysis. *arXiv preprint arXiv:1807.07994*, 2018.
- [40] A. Paszke, S. Gross, S. Chintala, G. Chanan, E. Yang, Z. DeVito, Z. Lin, A. Desmaison, L. Antiga, and A. Lerer. Automatic differentiation in pytorch. 2017.
- [41] V. Ramamurthy and N. Duffy. L-sr1: a second order optimization method. 2017.
- [42] N. M. P. L. Rates. Automatic and simultaneous adjustment of learning rate and momentum for stochastic gradient descent.
- [43] S. J. Reddi, S. Kale, and S. Kumar. On the convergence of adam and beyond. In *International Conference on Learning Representations*, 2018.
- [44] G. Ribière and E. Polak. Note sur la convergence de directions conjuguées. *Rev. Francaise Informat Recherche Opertionelle*, 16:35–43, 1969.
- [45] H. Robbins and S. Monro. A stochastic approximation method. *Annals of Mathematical Statistics*, 22:400–407, 1951.
- [46] M. Rolinek and G. Martius. L4: Practical loss-based stepsize adaptation for deep learning. In *Advances in Neural Information Processing Systems*, pages 6434–6444, 2018.
- [47] D. E. Rumelhart, G. E. Hinton, and R. J. Williams. Learning representations by back-propagating errors. *nature*, 323(6088):533, 1986.
- [48] M. Sandler, A. G. Howard, M. Zhu, A. Zhmoginov, and L.-C. Chen. Mobilenetv2: Inverted residuals and linear bottlenecks. *2018 IEEE/CVF Conference on Computer Vision and Pattern Recognition*, pages 4510–4520, 2018.
- [49] N. N. Schraudolph, J. Yu, and S. Găjnter. A stochastic quasi-newton method for online convex optimization. In M. Meila and X. Shen, editors, *Proceedings of the Eleventh International Conference on Artificial Intelligence and Statistics*, volume 2 of *Proceedings of Machine Learning Research*, pages 436–443, San Juan, Puerto Rico, 21–24 Mar 2007. PMLR.
- [50] K. Simonyan and A. Zisserman. Very deep convolutional networks for large-scale image recognition. *CoRR*, abs/1409.1556, 2014.
- [51] N. Srivastava, G. Hinton, A. Krizhevsky, I. Sutskever, and R. Salakhutdinov. Dropout: A simple way to prevent neural networks from overfitting. *Journal of Machine Learning Research*, 15:1929–1958, 2014.
- [52] M. Tan and Q. V. Le. Efficientnet: Rethinking model scaling for convolutional neural networks. In *ICML*, 2019.
- [53] T. Tieleman and G. Hinton. Lecture 6.5-rmsprop, coursera: Neural networks for machine learning. *University of Toronto, Technical Report*, 2012.
- [54] S. Vaswani, A. Mishkin, I. Laradji, M. Schmidt, G. Gidel, and S. Lacoste-Julien. Painless stochastic gradient: Interpolation, line-search, and convergence rates. *arXiv preprint arXiv:1905.09997*, 2019.
- [55] C. Xing, D. Arpit, C. Tsirigotis, and Y. Bengio. A walk with SGD. *arXiv preprint arXiv:1802.08770*, 2018.
- [56] Y. Yamada, M. Iwamura, T. Akiba, and K. Kise. Shakedrop regularization for deep residual learning. 2018.
- [57] E. Yudkowsky et al. Artificial intelligence as a positive and negative factor in global risk. *Global catastrophic risks*, 1(303):184, 2008.
- [58] M. D. Zeiler. Adadelta: An adaptive learning rate method. *CoRR*, abs/1212.5701, 2012.

A Further line plots

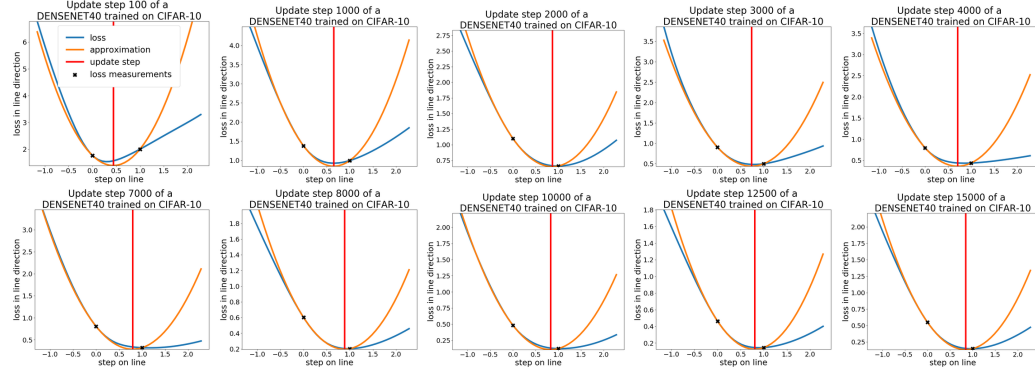


Figure 7: **DenseNet40** loss functions on lines in negative gradient direction (blue) combined with their parabolic approximation (orange) and the position of the minimum (red). The unit of the horizontal axis is the change of θ .

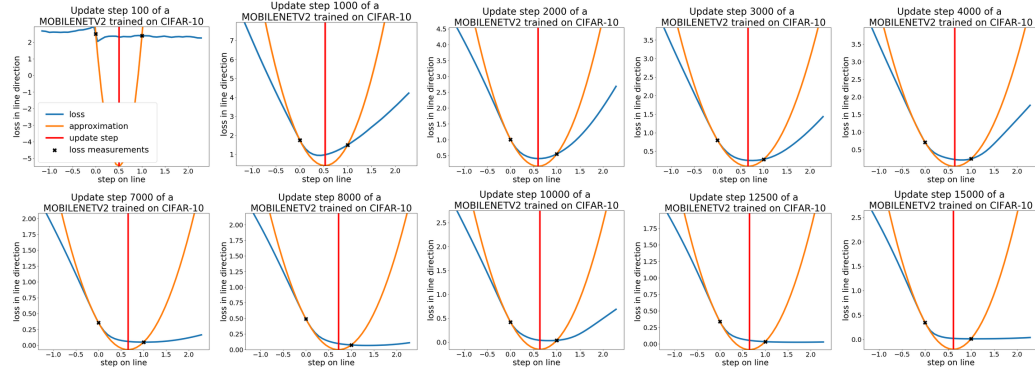


Figure 8: Loss line plots for **MobileNetV2**. For explanations see Figure 8. During training the parabolic approximation fits less accurately on the right hand side, however, the minimum of the parabola is still a good estimator for a low loss value on the line

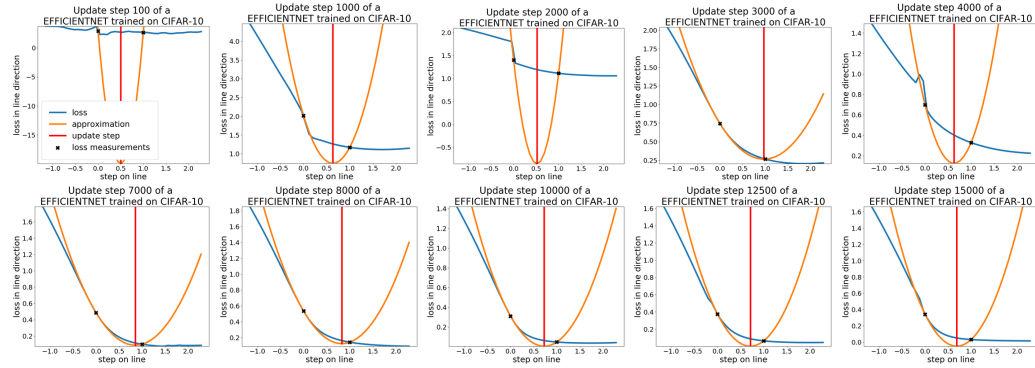


Figure 9: Loss line plots for **EfficientNet**. For explanations see Figure 8. The parabolic approximation fits only on the left hand side, however, the minimum of the parabola is still a good estimator for a low loss value on the line

B PAL with all additions:

Algorithm 2 provides the full implementation of *PAL* including the additions described in Section 4.3. After analyzing the best hyperparameter combinations of *PAL* over all experiments, we suggest to use values from the following parameter intervals: $\mu = [0.1, 1]$, $\alpha = [1.0, 1.6]$, $\beta = [0, 0.4]$, $s_{max} = [3]$. Where α, β and s_{max} usually have a low sensitivity. Thus, the basic implementation of *PAL* (Algorithm 1) performs already well and is always found in the upper quartile considering the performance of all analyzed hyperparameter configurations in our experiments. PyTorch and Tensorflow implementations are provided at <https://github.com/cogsys-tuebingen/PAL>.

Algorithm 2 *PAL*, our proposed line search algorithm for DNNs. See Section 4 for details.

<p>Input: Hyperparameters: μ: measuring step size, α: update step adaptation, β: conjugate gradient factor, s_{max}: maximum step size.</p> <p>Input: $L(x; \theta)$: loss function</p> <p>Input: x: list of input vectors</p> <p>Input: θ_0: initial parameter vector</p> <p>1: $t \leftarrow 0$</p> <p>2: $d_t \leftarrow \vec{0}$</p> <p>3: while θ_t not converged do</p> <p>4: $l_0 \leftarrow L(x_t; \theta_t)$</p> <p>5: $d_t \leftarrow -\nabla_{\theta_t} L(x_t; \theta_t) + \beta d_{t-1}$</p> <p>6: $l_\mu \leftarrow L(x_t; \theta_t + \mu \frac{d_t}{\ d_t\ })$</p> <p>7: $b \leftarrow \nabla_{\theta_t} L(x_t; \theta_t) \frac{d_t}{\ d_t\ }$</p> <p>8: $a \leftarrow \frac{l_\mu - l_0 - b\mu}{\mu^2}$</p>	<p>9: if $a > 0$ and $b < 0$ then</p> <p>10: $s_{upd} \leftarrow -\alpha \frac{b}{2a}$</p> <p>11: else if $a \leq 0$ and $b < 0$ then</p> <p>12: $s_{upd} \leftarrow \mu$</p> <p>13: else</p> <p>14: $s_{upd} \leftarrow 0$</p> <p>15: end if</p> <p>16: if $s_{upd} > s_{max}$ then</p> <p>17: $s_{upd} \leftarrow s_{max}$</p> <p>18: end if</p> <p>19: $\theta_{t+1} \leftarrow \theta_t + s_{upd} \frac{d_t}{\ d_t\ }$</p> <p>20: $t \leftarrow t + 1$</p> <p>21: end while</p> <p>22: return θ_t</p>
---	---

C Proofs

Lemma 1. Let $f : \mathbb{R}^n \rightarrow \mathbb{R}$ a k -times continuously differentiable function. Furthermore, assume there exists $a, b, c \in \mathbb{R}$ with $a > 0$, such that $f(\mathbf{l} + \mathbf{d}s) = as^2 + bs + c$ for all $s \in \mathbb{R}$. Then there exist $z \in \mathbb{R}$, $\mathbf{r} \in \mathbb{R}^n$ and a positive definite Matrix $\mathbf{Q} \in \mathbb{R}^{n \times n}$ such that $f(\mathbf{x}) = c + \mathbf{r}^T \mathbf{x} + \mathbf{x}^T \mathbf{Q} \mathbf{x}$ for all $\mathbf{x} \in \mathbb{R}^n$.

Proof.

$$g(\mathbf{x}) = u + \mathbf{v}^T \mathbf{x} + \mathbf{x}^T \mathbf{W} \mathbf{x} \text{ for some } u \in \mathbb{R}, \mathbf{v} \in \mathbb{R}^n \text{ and } \mathbf{W} \in \mathbb{R}^{n \times n}$$

$$\Leftrightarrow \forall \mathbf{l}, \mathbf{d} \in \mathbb{R}^n \wedge \|\mathbf{d}\| = 1 : \sum_{j=1}^n \sum_{k=1}^n \sum_{l=1}^n \frac{\partial^3 g(\mathbf{l})}{\partial x_j \partial x_k \partial x_l} d_j d_k d_l = 0 \quad (5)$$

\Rightarrow holds since we have a polynomial of degree 2 and its third derivative is always a $\mathbf{0}$ tensor.

\Leftarrow holds since the remainder of the quadratic Taylor expansion is always 0.

In our case the right part is 0 since:

$$\sum_{j=1}^n \sum_{k=1}^n \sum_{l=1}^n \frac{\partial^3 f(\mathbf{l})}{\partial x_j \partial x_k \partial x_l} d_j d_k d_l = \frac{\partial}{\partial s^3} f(\mathbf{l} + \mathbf{d}s) = 0 \quad (6)$$

In words: $f(\mathbf{x})$ is a parabolic function if and only if for each location \mathbf{l} the third directional derivative of $f(\mathbf{l})$ in each direction \mathbf{d} is 0. Which is the case, since the third derivative of each intersection is 0. \mathbf{W} is positive definite since:

$$\forall \mathbf{d}, \mathbf{l} \in \mathbb{R}^n \wedge \|\mathbf{d}\| = 1 : \mathbf{d}^T \mathbf{W} \mathbf{d} = \frac{1}{2} \mathbf{d}^T \mathbf{H}(\mathbf{l}) \mathbf{d} = \frac{1}{2} \frac{\partial}{\partial s^2} f(\mathbf{l} + \mathbf{d}s) = a > 0 \quad (7)$$

where \mathbf{H} is the Hessian. ■

Proposition 1. *PAL converges on $f(\mathbf{x}) : \mathbb{R}^n \rightarrow \mathbb{R}, f(\mathbf{x}) = c + \mathbf{r}^T \mathbf{x} + \mathbf{x}^T \mathbf{Q} \mathbf{x}$ with $\mathbf{Q} \in \mathbb{R}^{n \times n}$ hermitian and positive definite.*

Proof.

For this prove we consider a basic *PAL* without the features introduced in Section 4.3. Note, that during the proof we will see, that $a > 0$ and $b < 0$. Thus, only the update step for this case has to be considered (see Section 4.2).

$f(\mathbf{x})$ is convex since \mathbf{Q} is positive definite. Thus it has one minimum.
Without loss of generality we set $c = 0, \mathbf{r} = \mathbf{0}, \mathbf{x}_n \neq \mathbf{0}$

$$f(\mathbf{x}) = \mathbf{x}^T \mathbf{Q} \mathbf{x} \text{ and } \nabla_{\mathbf{x}} f(\mathbf{x}) = f'(\mathbf{x}) = 2\mathbf{Q} \mathbf{x} \quad (8)$$

The values of $f(x)$ along a line through \mathbf{x} in the direction of $-f'(\mathbf{x})$ are given by:

$$f(-f'(\mathbf{x})\hat{s} + \mathbf{x}) \quad (9)$$

Now we expand the line function:

$$\begin{aligned} f(-f'(\mathbf{x})\hat{s} + \mathbf{x}) &= f(-2\mathbf{Q}\mathbf{x}\hat{s} + \mathbf{x}) \\ &= (-2\mathbf{Q}\mathbf{x}\hat{s} + \mathbf{x})^T \mathbf{Q} (-2\mathbf{Q}\mathbf{x}\hat{s} + \mathbf{x}) \\ &= \underbrace{4\mathbf{x}^T \mathbf{Q}^3 \mathbf{x} \hat{s}^2}_{=:a} + \underbrace{-4\mathbf{x}^T \mathbf{Q}^2 \mathbf{x} \hat{s}}_{=:b} + \underbrace{\mathbf{x}^T \mathbf{Q} \mathbf{x}}_{=:c} \end{aligned} \quad (10)$$

Here we see that $f(\hat{s})$ is indeed a parabolic function with $a > 0, b < 0$ and $c > 0$ since $\mathbf{Q}^3, \mathbf{Q}^2$ and \mathbf{Q} are positive definite.

The location of the minimum s_{min} of $f(\hat{s})$ is given by:

$$\hat{s}_{min} = \arg \min_{\hat{s}} f(-f'(\mathbf{x})\hat{s} + \mathbf{x}) = -\frac{b}{2a} \quad (11)$$

PAL determines \hat{s}_{min} exactly with $\hat{s}_{min} = \frac{s_{upd}}{\|f'(x)\|}$ (see equation 1 and 2). $\|f'(x)\| > 0$ since otherwise we are already in the minimum.

The value at the minimum is given by:

$$f(\hat{s}_{min}) = a\left(\frac{-b}{2a}\right)^2 + b\left(\frac{-b}{2a}\right) + c = -\frac{b^2}{4a} + c = -\underbrace{\frac{(-\mathbf{x}^T \mathbf{Q}^2 \mathbf{x})^2}{\mathbf{x}^T \mathbf{Q}^3 \mathbf{x}}}_{=:g(\mathbf{x})} + \mathbf{x}^T \mathbf{Q} \mathbf{x} = -g(\mathbf{x}) + f(\mathbf{x}) \quad (12)$$

Since \mathbf{Q}^2 and \mathbf{Q}^3 are positive definite and $\mathbf{x} \neq \mathbf{0}$:

$$g(\mathbf{x}) > 0 \quad (13)$$

Now we consider the sequence $f(\mathbf{x}_n)$, with \mathbf{x}_n defined by *PAL* (see Equation 1):

$$\mathbf{x}_{n+1} = -\frac{f'(\mathbf{x}_n)}{\|f'(\mathbf{x}_n)\|} \hat{s}_{upd} + \mathbf{x}_n = -f'(\mathbf{x}_n) \hat{s}_{min} + \mathbf{x}_n \quad (14)$$

It is easily seen by induction that:

$$0 < f(\mathbf{x}_{n+1}) < f(\mathbf{x}_n) = \sum_{i=0}^{n-1} -g(\mathbf{x}_i) + f(\mathbf{x}_0) < f(\mathbf{x}_0). \quad (15)$$

$g(\mathbf{x}_n)$ converges to 0. Since $\forall n : g(\mathbf{x}_n) > 0$ and $\sum_{i=0}^{n-1} -g(\mathbf{x}_i)$ is bounded.

Now we have to show that \mathbf{x}_n converges to 0.

We have:

$$g(\mathbf{x}_n) = \frac{(\mathbf{x}_n^T \mathbf{Q}^2 \mathbf{x}_n)^2}{\mathbf{x}_n^T \mathbf{Q}^3 \mathbf{x}_n} = \frac{\langle \mathbf{x}_n, \mathbf{Q}^2 \mathbf{x}_n \rangle^2}{\langle \mathbf{x}_n, \mathbf{Q}^3 \mathbf{x}_n \rangle} \quad (16)$$

Now we use the theorem of Courant-Fischer:

$$\langle x, x \rangle \min\{\lambda_1, \dots, \lambda_n\} \leq \langle x, Ax \rangle \leq \langle x, x \rangle \max\{\lambda_1, \dots, \lambda_n\} \quad (17)$$

for any symmetric $A \in \mathbb{R}^{n \times n}$ with $\lambda_1, \dots, \lambda_n$

And get:

$$g(\mathbf{x}_n) \geq \frac{\lambda_{\mathbf{Q}^2 \min}^2 \langle \mathbf{x}_n, \mathbf{x}_n \rangle^2}{\lambda_{\mathbf{Q}^3 \max} \langle \mathbf{x}_n, \mathbf{x}_n \rangle} = C \frac{\|\mathbf{x}_n\|^4}{\|\mathbf{x}_n\|^2} = C \|\mathbf{x}_n\|^2 \quad (18)$$

with

$$C = \frac{\lambda_{\mathbf{Q}^2 \min}^2}{\lambda_{\mathbf{Q}^3 \max}} > 0 \text{ since all } \lambda \text{ of the positive definite } \mathbf{Q} \text{ are positive} \quad (19)$$

Thus, we have:

$$g(\mathbf{x}_n) \geq C \|\mathbf{x}_n\|^2 \geq 0 \quad (20)$$

Since $g(\mathbf{x}_n)$ converges to 0, $C \|\mathbf{x}_n\|^2$ converges to 0.

This means, \mathbf{x}_n converges to $\mathbf{0}$, which is the location of the minimum. ■

Proposition 2. If $\mathcal{L}(\theta) : \mathbb{R}^n \rightarrow \mathbb{R} \theta \mapsto \mathcal{L}(\theta) = \frac{1}{m} \sum_{i=1}^m c_i + \mathbf{r}_i^T \theta + \theta^T \mathbf{Q}_i \theta$ and $c_i + \mathbf{r}_i^T \theta + \theta^T \mathbf{Q}_i \theta = L(\theta; \mathbf{x}_i)$ with m being number the of batches and \mathbf{x}_i defining one batch. (Each batch defines a parabola. The empirical loss $\mathcal{L}(\theta)$ is the mean of these parabolas). And for all $i, j \in \mathbb{N}$ it holds that $\mathbf{Q}_i = \mathbf{Q}_j$ and that \mathbf{Q}_i is positive definite. Then $\arg \min_{\theta} \mathcal{L}(\theta) = \frac{1}{m} \sum_{i=1}^m \arg \min_{\theta} L(\theta)$ holds.

Proof.

Since $\mathcal{L}(\theta)$ is a sum of convex functions, it is also convex and has one minimum.

At first we determine the derivative of $\mathcal{L}(\theta)$ with respect to θ :

$$\frac{\partial}{\partial \theta} \mathcal{L}(\theta) = \frac{1}{m} \sum_{i=1}^m (\mathbf{r}_i + 2\mathbf{Q}_i \theta) = 2\mathbf{Q} \theta + \frac{1}{m} \sum_{i=1}^m \mathbf{r}_i \quad (21)$$

Then we determine the minima:

$$\arg \min_{\theta} \mathcal{L}(\theta) \Leftrightarrow \frac{\partial}{\partial \theta} \mathcal{L}(\theta) = \mathbf{0} \Leftrightarrow \theta = -\frac{1}{2} \left(\sum_{i=1}^m \mathbf{Q}_i \right)^{-1} \sum_{i=1}^m \mathbf{r}_i = -\frac{1}{2m} \mathbf{Q}^{-1} \sum_{i=1}^m \mathbf{r}_i \quad (22)$$

$$\arg \min_{\mathbf{t}} L(\mathbf{t} : \mathbf{x}_i) = -\frac{1}{2} \mathbf{Q}^{-1} \mathbf{r}_i \quad (23)$$

Thus, we get:

$$\arg \min_{\theta} \mathcal{L}(\theta) = -\frac{1}{2m} \mathbf{Q}^{-1} \sum_{i=1}^m \mathbf{r}_i = \frac{1}{m} \sum_{i=1}^m -\frac{1}{2} \mathbf{Q}^{-1} \mathbf{r}_i = \frac{1}{m} \sum_{i=1}^m \arg \min_{\mathbf{t}} L(\mathbf{t} : \mathbf{x}_i) \quad (24)$$

■

D Further experimental results

D.1 Performance Comparison on ImageNet, CIFAR-10, CIFAR-100 and Tolstoi

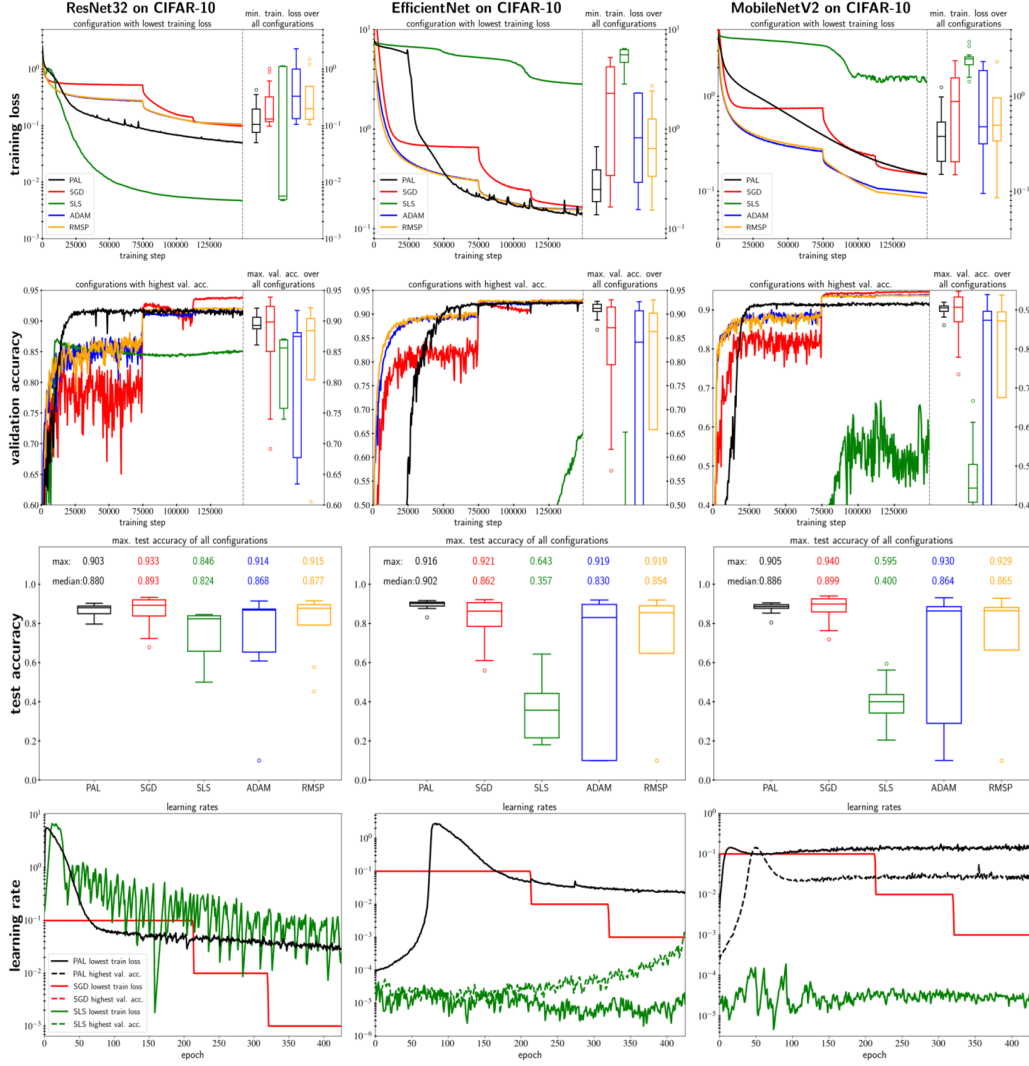


Figure 10: Fair comparison on **CIFAR-10** of **PAL** against **SLS**, **SGD**, **ADAM**, **RMSProp** on training loss (row 1), validation accuracy (row 2), test accuracy (row 3) and **SLS**, **SGD** and **PAL** on learning rates (row 4). Results are averaged over 3 runs. Box plots result from comprehensive hyperparameter grid searches in plausible intervals. **PAL** competes against all other optimizers except against **SGD**. The learning rate schedule comparison shows that **PAL** performs competitive although elaborating significantly different schedules.

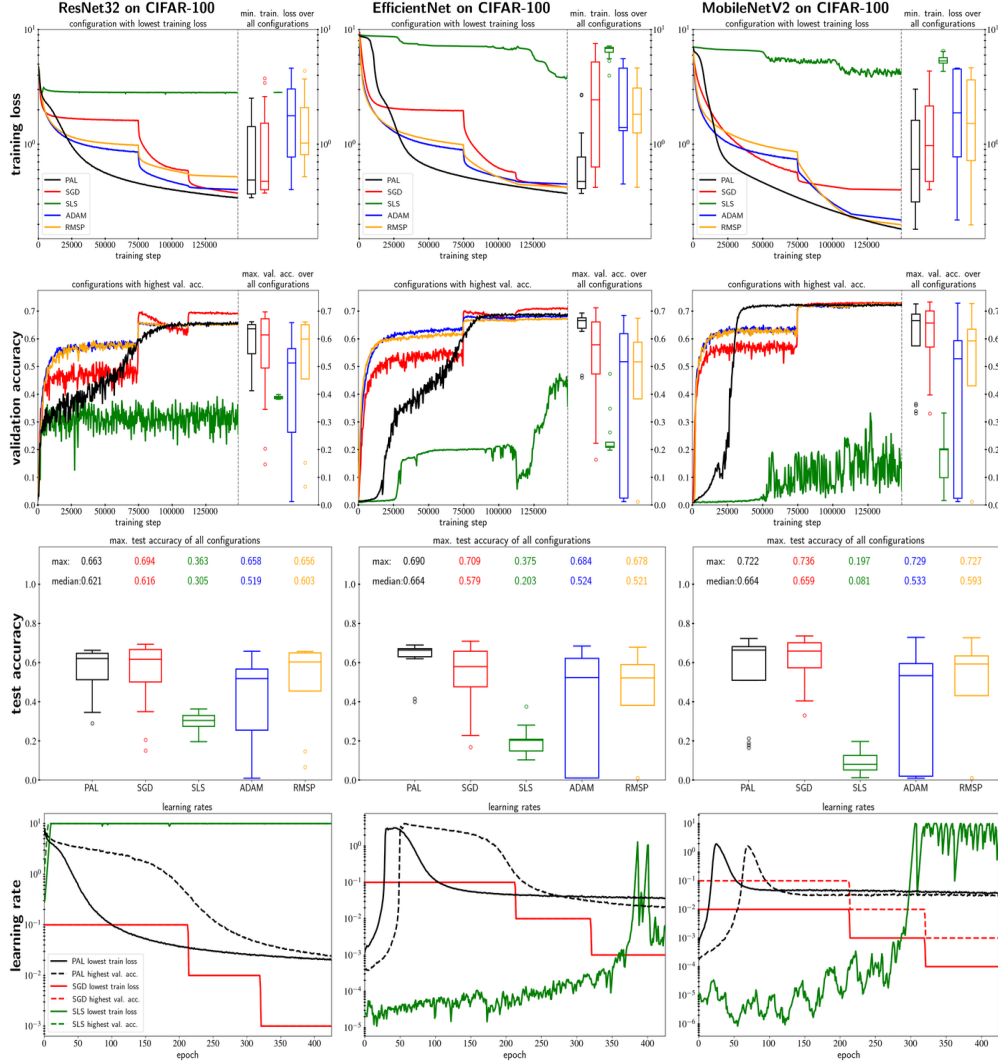


Figure 11: Fair comparison on **CIFAR-100** of *PAL* against *SLS*, *SGD*, *ADAM*, *RMSProp* on training loss (row 1), validation accuracy (row 2), test accuracy (row 3) and *SLS*, *SGD* and *PAL* on learning rates (row 4). Results are averaged over 3 runs. Box plots result from comprehensive hyperparameter grid searches in plausible intervals. *PAL* competes against all other optimizers except against *SGD*. The learning rate schedule comparison shows that *PAL* performs competitive although elaborating significantly different schedules.

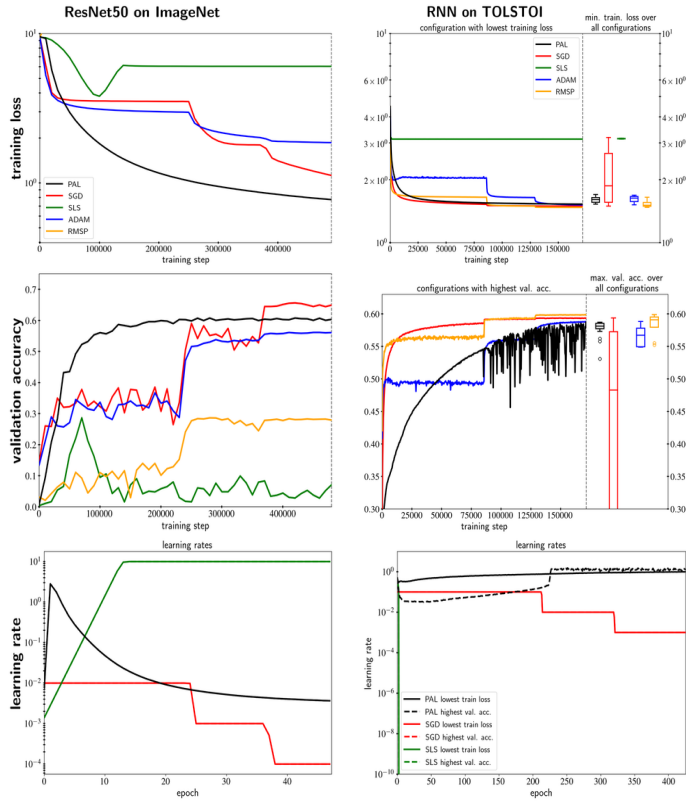


Figure 12: Comparison of *PAL* to *SGD*, *SLS*, *ADAM*, *RMSProp* on training loss, validation accuracy and learning rates on **Imagenet**, and a simple RNN, trained on the **Tolstoi** War and Peace dataset. For Imagenet the best hyperparameter configuration from the CIFAR-100 evaluation were used to test hyperparameter transferability.

D.2 Wall-clock time comparison

Table 1: Required seconds per epoch of *PAL*, *SLS* and *SGD* on CIFAR-10. RMSP and ADAM reach a similar speed as *SGD*. The comparison was performed on a Nvidia Geforce GTX 1080 TI.

network	seconds per epoch <i>PAL</i>	seconds per epoch <i>SLS</i>	seconds per epoch <i>SGD</i>	% <i>PAL</i> of <i>SLS</i>	% <i>PAL</i> of <i>SGD</i>
ResNet32	20.9	21.7	10.7	96.3%	194.3%
MobilenetV2	53.2	52.4	34.1	101.5%	155.8%
EfficientNet	55.5	52.2	30.7	106.3%	180.8%
DenseNet40	88.8	87.5	59.7	101.5%	148.7%

D.3 SLS ResNet34 test case re-implementation

In the shown experiments and in contrast to the evaluation of *SLS* in [54], we used Tensorflow default Xavier weight initialization [18] versus PyTorch default Lecun initialization [32]. In addition, we used L2 regularisation versus no regularization. Furthermore default implementations of networks for both frameworks have small differences. All in all those differences usually influence the optimizer performance only marginally as given by the fact that all other tested optimizers perform well. However, in this case of *SLS* we see significant differences.

To prove that our implementation of *SLS* is correct, we re-implemented [54]’s ResNet34 test case on CIFAR-10 in Tensorflow and achieved similar results as [54]. *SLS* shows well performance and is not significantly overfitting as it does in in Section 5.2

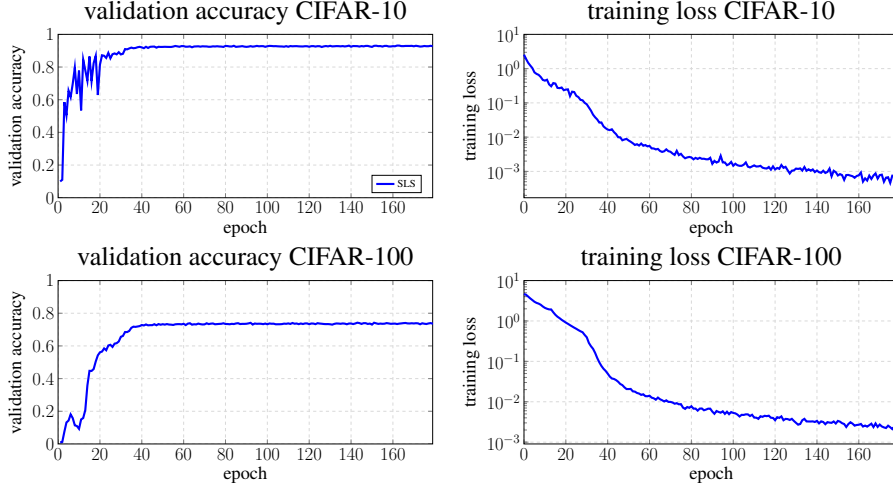


Figure 13: On the re-implemented ResNet34 test case of [54] *SLS* shows well performance and is not significantly overfitting as it does in in Section 5.2

D.4 Sensitivity analysis:

All in all *PAL* tends to have a low hyperparameter sensitivity as shown in Figure 14.

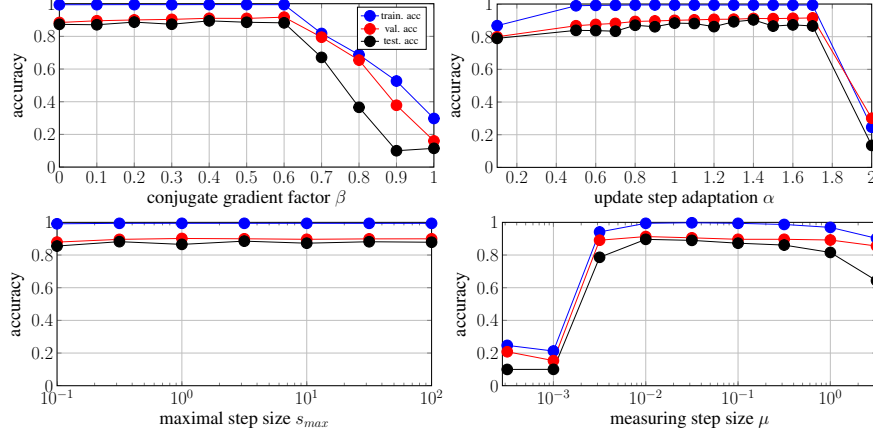


Figure 14: Sensitivity analysis for PAL on a ResNet32 trained on CIFAR-10. The baseline parameters are: $\mu = 0.1, \beta = 0.2, \alpha = 1.0, s_{max} = 10$. It shows that β should be chosen ≤ 0.6 . α has a low sensitivity, but with a value of 1.4 it reaches best performance. s_{max} has a low sensitivity and all investigated values perform similarly. μ should be chosen between 10^{-2} and $10^{-0.5}$.

D.5 Further experimental design details

D.5.1 Training Procedure

On CIFAR-10 and CIFAR-100 we trained 150k steps. On Imagenet each network was trained for 500k steps. We performed a piecewise constant learning rate decay by dividing the learning rate by 10 at 50% and 75% of the steps.

The training set to evaluation set split was 45k to 15k for CIFAR-10 and CIFAR-100. At the time of writing, the default Tensorflow classes do not support the reuse of the same randomly sampled numbers for multiple inferences, therefore, we implemented and used our own Dropout [51] layer. To get a fair comparison of the optimizers capabilities, we compare on the training loss, the validation accuracy and the test accuracy metrics. For all metrics we provide the median and the quartiles to analyze the hyperparameter sensitivity. For each hyperparameter combination we averaged our results over 3 runs using the seeds 1, 2 and 3 for reproducibility. All in all, we trained 1494 networks with Tensorflow 1.15 [1] on Nvidia Geforce GTX 1080 TI graphic cards.

D.5.2 Data Augmentation

On CIFAR-10 we performed the following augmentations [22]:

4 pixel padding and cropping, horizontal image flipping with probability 0.5.

On Imagenet we applied an initial random crop to 224x224 pixels. In addition, we applied lighting as described in [31]. For CIFAR-10, CIFAR-100 all images were normalized by channel-wise mean and variance. For the Tolstoi War and Peace dataset we omitted augmentation.

D.5.3 Hyperparameter grid search

For our evaluation we used all combinations out of the following common used hyperparameters. The batch size is always 128. Weight decay is always 10^{-4} . On Imagenet, such a large grid search was not possible. In this case we compared with the best hyperparameter combinations found on Cifar-100.

ADAM:

hyperparameter	symbol	values
learning rate	λ	$\{1, 0.1, 0.01, 0.001, 0.0001\}$
first momentum	β_1	$\{0.9, 0.95\}$
second momentum	β_2	$\{0.999\}$
epsilon	ϵ	$\{1e-8\}$

We did not vary the first or second momentum much, since [29] states that the values chosen are already good defaults.

SGD:

hyperparameter	symbol	values
learning rate	λ	$\{0.1, 0.01, 0.001, 0.0001\}$
momentum	α	$\{0.85, 0.9, 0.95\}$

RMSPProp:

hyperparameter	symbol	values
learning rate	λ	$\{0.1, 0.01, 0.001, 0.0001\}$
discounting factor	f	$\{0.9, 0.95\}$
epsilon	ϵ	$\{1e-8\}$

PAL:

hyperparameter	symbol	values
measuring step size	μ	$\{10^0, 10^{-0.5}, 10^{-0.1}, 10^{-0.15}\}$
conjugate gradient factor	β	$\{0, 0.4\}$
update step adaptation	α	$\{1, \frac{1}{0.8}\}$
maximum step size	s_{max}	$\{10^{0.5} (\approx 3.16)\}$

In our implementation we worked with a inverse update step adaptation $\gamma = \frac{1}{\alpha}$.

SLS:

hyperparameter	symbol	values
initial step size	μ	$\{0.1, 1\}$
step size decay	β	$\{0.9, 0.99\}$
step size reset	γ	$\{2.0, 2.5\}$
Armijo constant	c	$\{0.1, 0.01\}$
maximum step size	μ_{max}	$\{10.0\}$

D.6 Detailed numerical results

See table 2.

Table 2: Performance comparison of *PAL*, *RMSPProp*, *ADAM*, *RADAM* and *SGD*. All hyperparameter combinations given in Appendix D.5 were evaluated for each architecture. Results are averaged over 3 runs starting from different random seeds, except for training on ImageNet, for which results were not averaged. Note that tests on Imagenet were performed with the best hyperparameters found on CIFAR-100 to test the transferability of hyperparameters.

dataset	network	optimizer	training loss min	median; p25; p75	validation accuracy max	median; p25; p75	test accuracy max	median; p25; p75
CIFAR-10	EfficientNet	RMSP	0.154	0.637; 0.333; 1.261	0.93	0.864; 0.658; 0.902	0.919	0.854; 0.648; 0.889
		ADAM	0.155	0.818; 0.292; 2.275	0.926	0.841; 0.211; 0.907	0.919	0.83; 0.1; 0.896
		SLS	2.837	5.596; 4.681; 6.292	0.653	0.357; 0.211; 0.443	0.643	0.357; 0.216; 0.442
		SGD	0.165	2.287; 0.343; 4.221	0.93	0.872; 0.794; 0.915	0.921	0.862; 0.784; 0.906
		PAL	0.137	0.244 ; 0.186; 0.388	0.927	0.912 ; 0.906; 0.921	0.916	0.902 ; 0.889; 0.908
CIFAR-10	MobileNetV2	RMSP	0.085	0.493; 0.337; 0.918	0.938	0.872; 0.675; 0.895	0.929	0.865; 0.664; 0.882
		ADAM	0.095	0.477; 0.314; 1.861	0.939	0.874; 0.309; 0.896	0.93	0.864; 0.289; 0.886
		SLS	1.387	2.462; 2.011; 2.584	0.667	0.443; 0.407; 0.504	0.595	0.4; 0.343; 0.437
		SGD	0.149	0.878; 0.204; 1.552	0.947	0.907 ; 0.87; 0.933	0.94	0.899 ; 0.859; 0.925
		PAL	0.15	0.377 ; 0.205; 0.531	0.92	0.905; 0.896; 0.91	0.905	0.886; 0.877; 0.896
CIFAR-10	DenseNet40	RMSP	0.139	0.389; 0.252; 0.866	0.927	0.879; 0.739; 0.915	0.92	0.867; 0.717; 0.909
		ADAM	0.13	0.524; 0.272; 0.978	0.922	0.83; 0.631; 0.911	0.913	0.806; 0.605; 0.907
		SLS	0.048	0.096 ; 0.079; 0.171	0.911	0.904; 0.897; 0.905	0.901	0.893 ; 0.89; 0.897
		SGD	0.144	0.791; 0.394; 1.743	0.932	0.855; 0.537; 0.915	0.93	0.847; 0.528; 0.91
		PAL	0.085	0.189; 0.146; 0.303	0.925	0.908 ; 0.894; 0.919	0.916	0.882; 0.861; 0.9
CIFAR-10	ResNet32	RMSP	0.105	0.199; 0.129; 0.498	0.922	0.884; 0.804; 0.904	0.915	0.877; 0.792; 0.896
		ADAM	0.105	0.332; 0.133; 1.004	0.917	0.875; 0.677; 0.881	0.914	0.868; 0.654; 0.873
		SLS	0.005	0.006 ; 0.005; 0.827	0.871	0.856; 0.758; 0.869	0.846	0.824; 0.657; 0.839
		SGD	0.098	0.131; 0.118; 0.322	0.939	0.899 ; 0.85; 0.924	0.933	0.893 ; 0.838; 0.92
		PAL	0.05	0.105; 0.075; 0.195	0.921	0.893; 0.887; 0.906	0.903	0.88; 0.849; 0.888
CIFAR-100	DenseNet40	RMSP	0.332	1.222; 0.768; 1.961	0.716	0.583; 0.482; 0.634	0.712	0.588; 0.482; 0.631
		ADAM	0.308	1.031; 0.851; 2.633	0.715	0.601; 0.254; 0.64	0.712	0.599; 0.226; 0.641
		SLS	1.341	1.825; 1.443; 1.927	0.723	0.614; 0.585; 0.698	0.612	0.479; 0.422; 0.554
		SGD	0.331	0.707; 0.416; 2.148	0.751	0.633; 0.49; 0.709	0.753	0.634; 0.498; 0.708
		PAL	0.236	0.338 ; 0.275; 0.439	0.73	0.686 ; 0.661; 0.705	0.717	0.676 ; 0.642; 0.695
CIFAR-100	EfficientNet	RMSP	0.422	1.823; 1.253; 2.968	0.675	0.517; 0.383; 0.588	0.678	0.521; 0.382; 0.59
		ADAM	0.45	1.394; 1.312; 4.606	0.684	0.518; 0.025; 0.619	0.684	0.524; 0.01; 0.621
		SLS	3.731	6.713; 6.348; 6.857	0.474	0.212; 0.208; 0.227	0.375	0.203; 0.149; 0.208
		SGD	0.42	2.44; 0.633; 5.214	0.712	0.579; 0.473; 0.661	0.709	0.579; 0.476; 0.658
		PAL	0.372	0.471 ; 0.409; 0.772	0.693	0.666 ; 0.638; 0.676	0.69	0.664 ; 0.63; 0.671
CIFAR-100	MobileNetV2	RMSP	0.198	1.518; 0.718; 3.368	0.728	0.593; 0.43; 0.635	0.727	0.593; 0.431; 0.634
		ADAM	0.218	1.873; 0.776; 4.524	0.729	0.528; 0.025; 0.593	0.729	0.533; 0.02; 0.595
		SLS	3.857	5.086; 5.031; 5.64	0.332	0.2; 0.099; 0.203	0.197	0.081; 0.052; 0.126
		SGD	0.4	0.974; 0.473; 2.151	0.733	0.657; 0.57; 0.7	0.736	0.659; 0.573; 0.701
		PAL	0.181	0.602 ; 0.314; 1.571	0.726	0.666 ; 0.574; 0.689	0.722	0.664 ; 0.509; 0.681
CIFAR-100	ResNet32	RMSP	0.519	1.019; 0.807; 2.083	0.661	0.599; 0.455; 0.651	0.656	0.603; 0.455; 0.65
		ADAM	0.402	1.772; 0.768; 3.038	0.659	0.513; 0.262; 0.564	0.658	0.519; 0.255; 0.567
		SLS	2.62	2.808; 2.78; 2.82	0.399	0.388; 0.384; 0.392	0.363	0.305; 0.274; 0.33
		SGD	0.375	0.474 ; 0.4; 1.522	0.697	0.614; 0.494; 0.672	0.694	0.616; 0.502; 0.667
		PAL	0.339	0.485; 0.369; 1.424	0.662	0.636 ; 0.546; 0.652	0.663	0.621 ; 0.512; 0.647
Tolstoi	RNN	RMSP	1.475	1.509 ; 1.492; 1.556	0.599	0.591 ; 0.579; 0.595	0.592	0.583 ; 0.572; 0.587
		ADAM	1.516	1.655; 1.596; 1.681	0.588	0.567; 0.55; 0.578	0.581	0.561; 0.543; 0.571
		SLS	3.128	3.149; 3.136; 3.156	0.169	0.159; 0.158; 0.165	0.168	0.158; 0.157; 0.164
		SGD	1.496	1.872; 1.56; 2.675	0.594	0.483; 0.278; 0.573	0.587	0.476; 0.275; 0.566
		PAL	1.528	1.569; 1.547; 1.588	0.587	0.581; 0.577; 0.586	0.579	0.571; 0.556; 0.575
Imagenet	ResNet50	RMSP	9.485	—	0.286	—	0.28	—
		ADAM	1.863	—	0.562	—	0.559	—
		SLS	3.808	—	0.286	—	0.069	—
		SGD	1.123	—	0.656	—	0.65	—
		PAL	0.773	—	0.608	—	0.608	—
Imagenet	DenseNet121	RMSP	6.901	—	0.0	—	0.0	—
		ADAM	6.901	—	0.001	—	0.0	—
		SLS	7.768	—	0.001	—	0.001	—
		SGD	3.308	—	0.458	—	0.452	—
		PAL	1.228	—	0.617	—	0.611	—

E Binary Line Search

The optimal binary line search we compared *PAL* against. Since the line decreases in negative gradient direction, at first a extrapolation phase performs as many steps forward as the loss does not increase. Afterwards a binary search is performed. This approach is valid if the underlying line is convex. For simple readability we chose Python 3.6 syntax.

```
Input: max_num_of_search_steps 1
def binary_line_search(last_loss, step, counter, is_extrapolate): 2
    if counter == max_num_of_search_steps: 3
        return last_loss 4
    counter += 1 5
    if is_extrapolate: 6
        current_loss = do_step_on_line(step) 7
        if current_loss < last_loss: 8
            return binary_line_search(current_loss, step, counter, 9
                                     is_extrapolate)
        else: 10
            is_extrapolate = False 11
            do_step_on_line(-step, get_loss=False) 12
    if not is_extrapolate: 13
        loss_right = do_step_on_line(0.5*step, True) 14
        if loss_right < last_loss: 15
            return binary_line_search(loss_right, 16
                                     0.5*step, counter, is_extrapolate)
        loss_left = do_step_on_line(-1*step, True) 17
        if loss_left < last_loss: 18
            return binary_line_search(loss_left, 19
                                     0.5*step, counter, is_extrapolate)
        do_step_on_line(0.5*step, get_loss=False) 20
        if loss_right >= last_loss and loss_left >= last_loss: 21
            return binary_line_search(loss_left, 0.5*step, 22
                                     counter, is_extrapolate)
        else: 23
            # this state is not possible 24
```